Supplementary Material

Stability improvement of the Pt/TiO_2 photocatalyst during photocatalytic pure water splitting

Xinyi Zhang,[a,c] Chunling Bo,[a,c] Shuang Cao,[a] Zhijie Cheng,[a] Zhaozhong Xiao,[a] Xiaolong Liu,[a] Ting Tan [a,*] and Lingyu Piao [a,b,*]

[a] *National Center for Nanoscience and Technology, Beijing 100190, China*

[b] *Center of Materials Science and Optoelectronics Engineering, University of Chinese Academy of Sciences, Beijing 100049, China*

[c] *University of Chinese Academy of Sciences, Beijing 100049, China*

*Corresponding author.

E-mail address: tant@nanoctr.cn (T. Tan), piaoly@nanoctr.cn (L. Piao).

TABLE OF CONTENTS

S1. Supplementary Figures

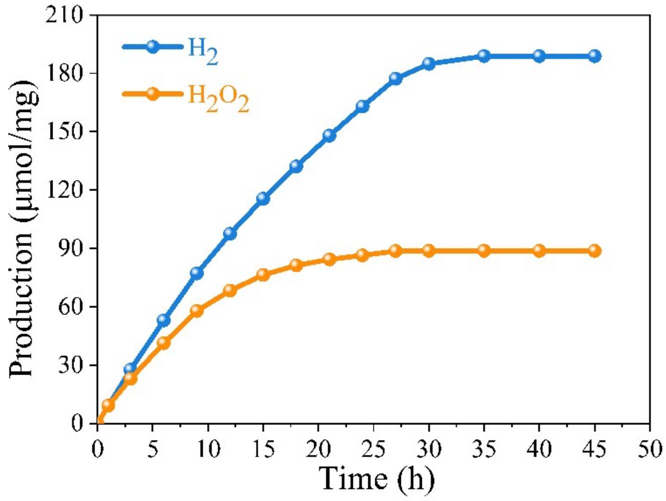

Fig. S1 The single stability of the Pt/b-TiO_2 NFs photocatalyst.

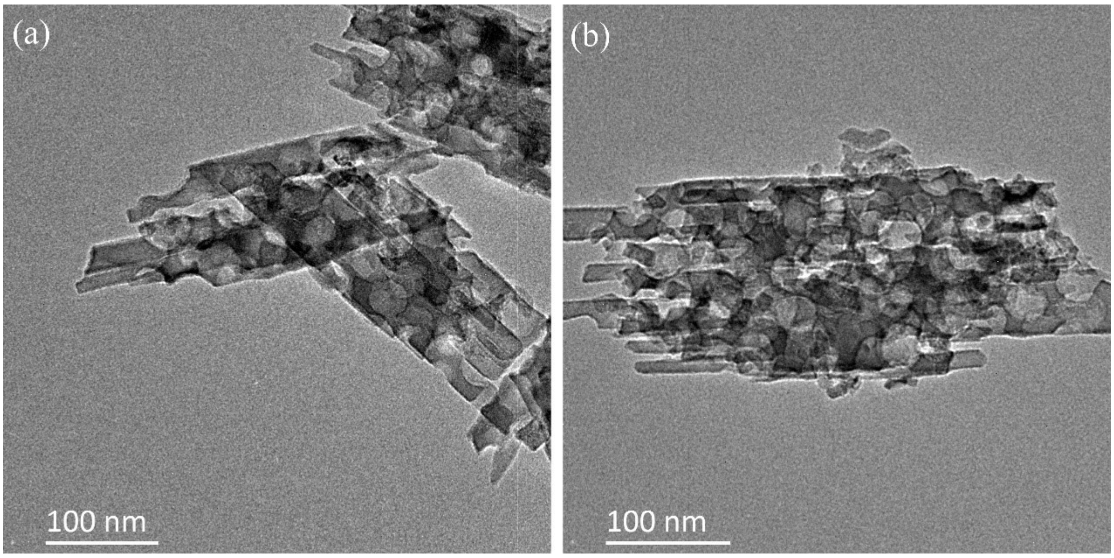

Fig. S2 TEM images of the Pt/b-TiO_2 NFs，(a) and (b) show the photocatalyst after 20 h and 40 h reaction, respectively.

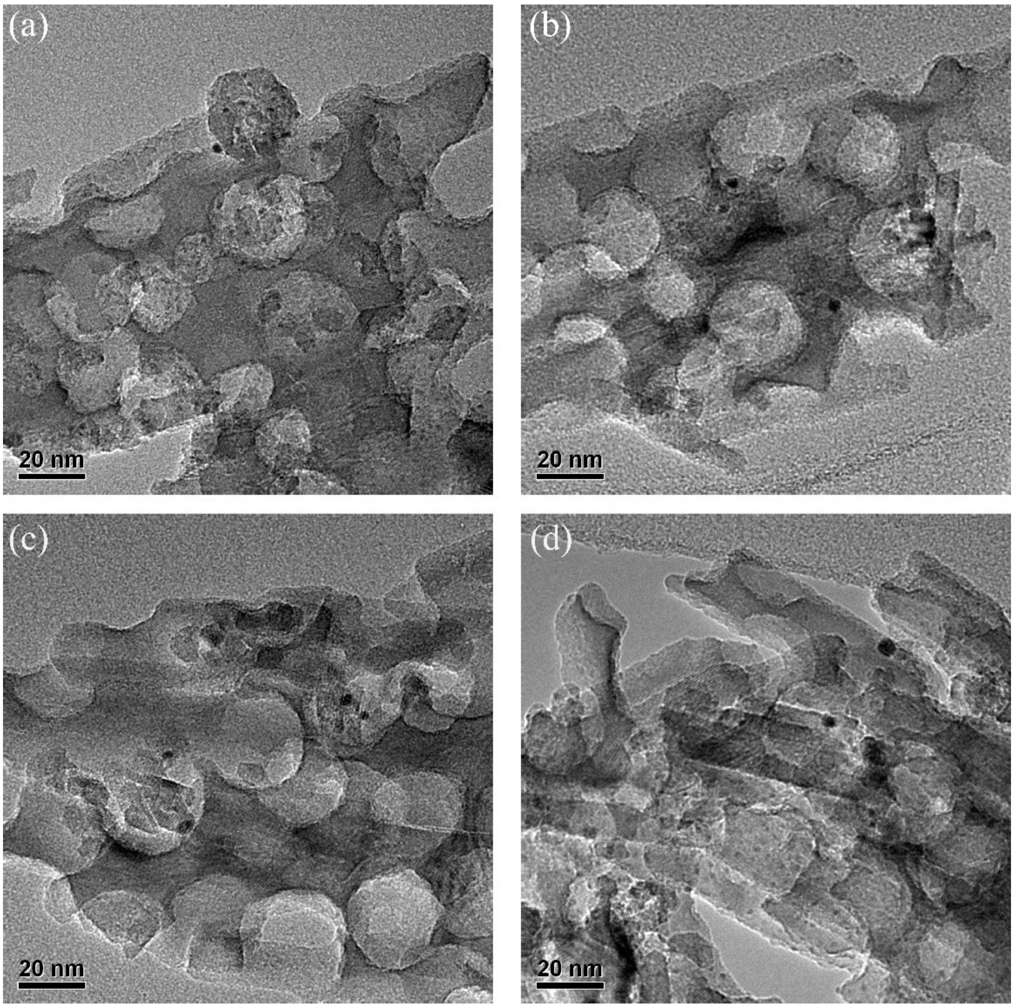

Fig. S3 (a), (b), (c), and (d) are the TEM images with higher resolution of the Pt/b-TiO_2 NFs after reaction for 0 h, 1 h, 20 h, and 40 h, respectively.

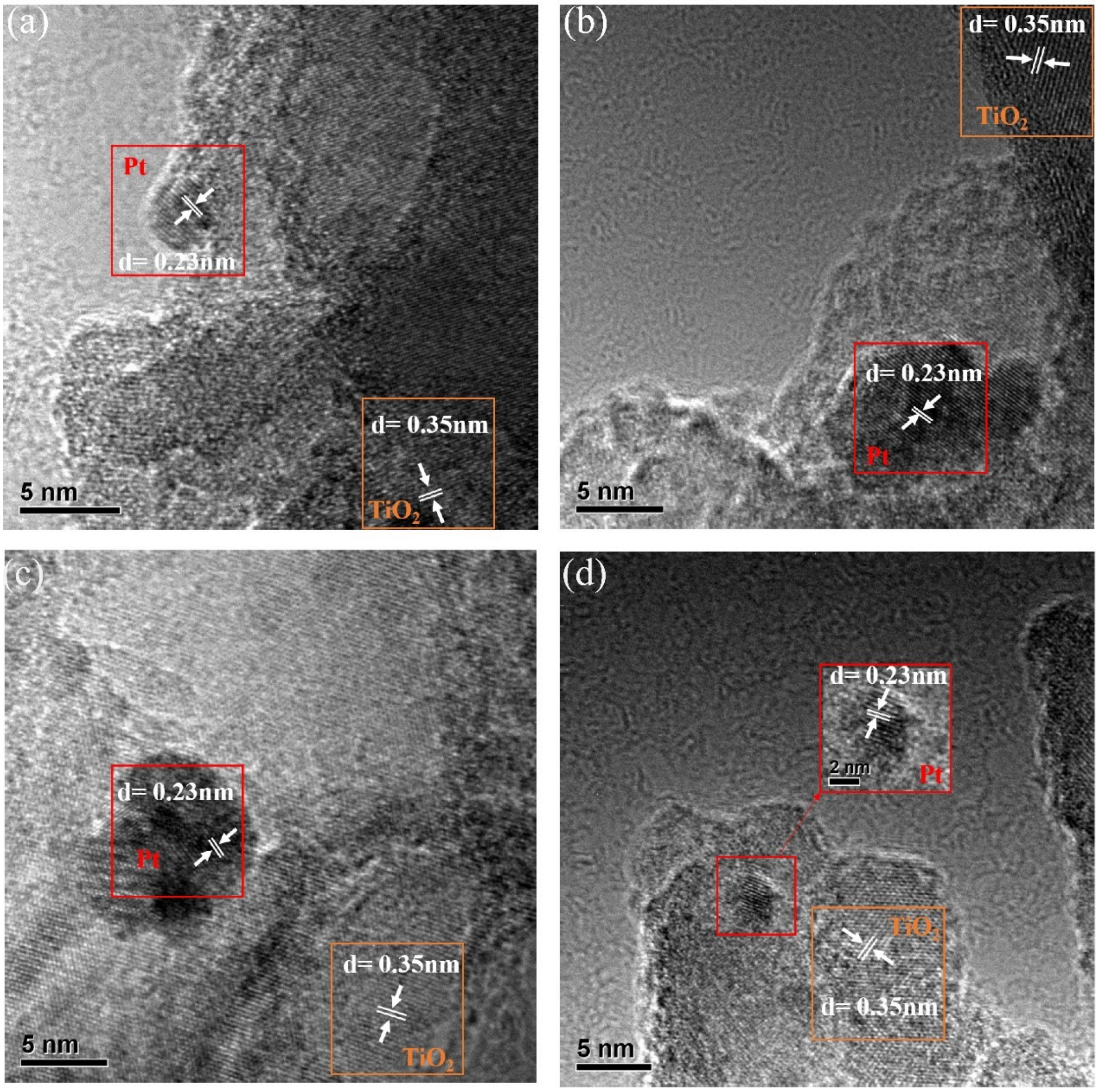

Fig. S4 (a), (b), (c), and (d) are the HRTEM images of the Pt/b-TiO_2 NFs after reaction for 0 h, 1 h, 20 h, and 40 h, respectively.

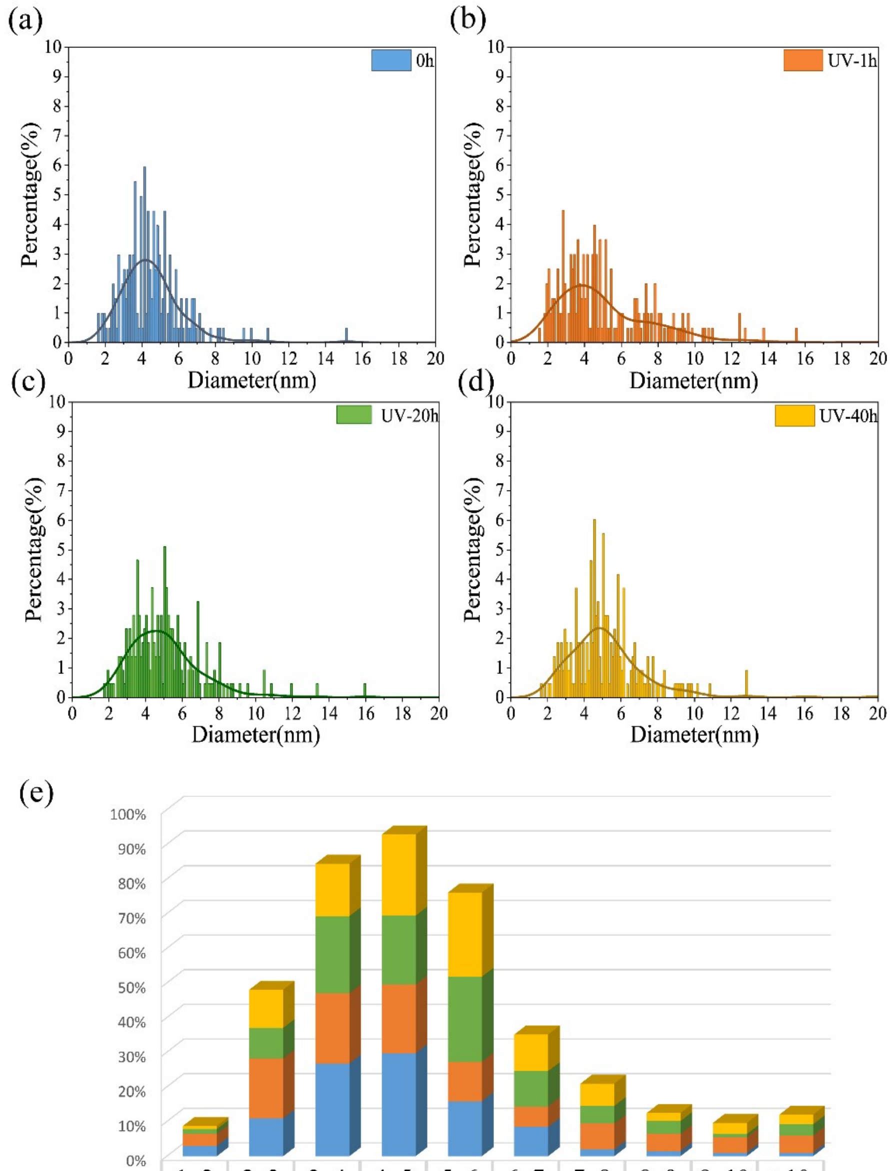

	1~2	2~3	3~4	4~5	5~6	6~7	7~8	8~9	9~10	>10
UV-40h	1%	11%	15%	23%	24%	11%	6%	2%	3%	3%
UV-20h	1%	9%	22%	20%	25%	10%	5%	4%	1%	3%
UV-1h	3%	17%	20%	20%	11%	6%	7%	5%	4%	5%
0h	3%	11%	27%	30%	16%	8%	2%	1%	1%	1%

Fig. S5 (a), (b), (c), (d) are the statistical histogram of Pt nanoparticles size distribution after reaction for 0 h, 1 h, 20 h, and 40 h, respectively. (e) Statistical chart of Pt particle size percentage after the reaction for 0 h, 1 h, 20 h, and 40h.

The average dimensions (a) of 5.0 ± 1.7 nm (Mean of N = 200 measurements, ± SD) are Pt before the reaction (0h). And 5.2 ± 2.7 nm (b), 5.1 ± 2.3 nm (c), and 5.3 ± 2.3 nm (d) are average dimensions of Pt nanoparticles after the reaction for 1 h, 20 h, and 40 h, respectively. Particle sizes are all concentrated at 4~6 nm (Fig. S3e), and there is no obvious change before and after the reaction.

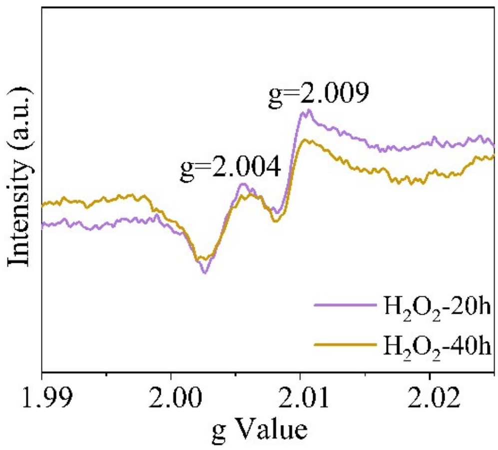

Fig. S6 EPR spectra of the Pt/b-TiO_2 NFs soaked in H_2O_2 for 20 h and 40 h, respectively.

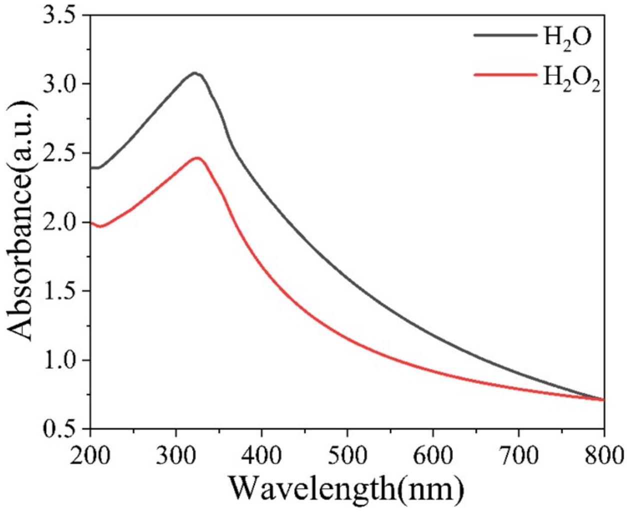

Fig. S7 UV-Vis absorption spectra of the Pt/b-TiO_2 NFs immersed in H_2O and H_2O_2. The H_2O_2 concentration here is the same as the H_2O_2 concentration under reaction conditions.

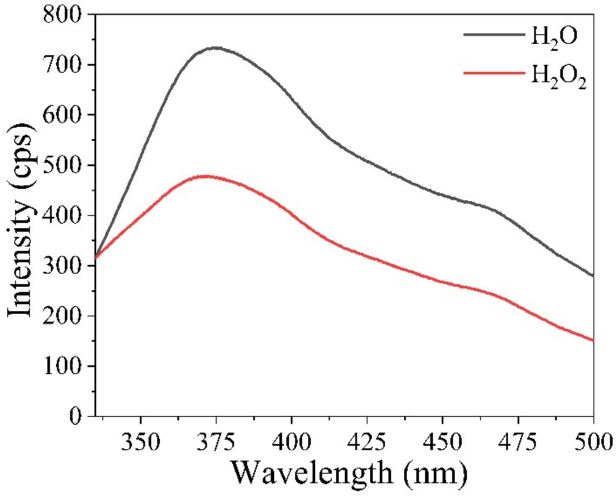

Fig. S8 Photoluminescence emission spectra of the Pt/b-TiO_2 NFs immersed in H_2O and H_2O_2. The H_2O_2 concentration here is the same as the H_2O_2 concentration under reaction conditions.

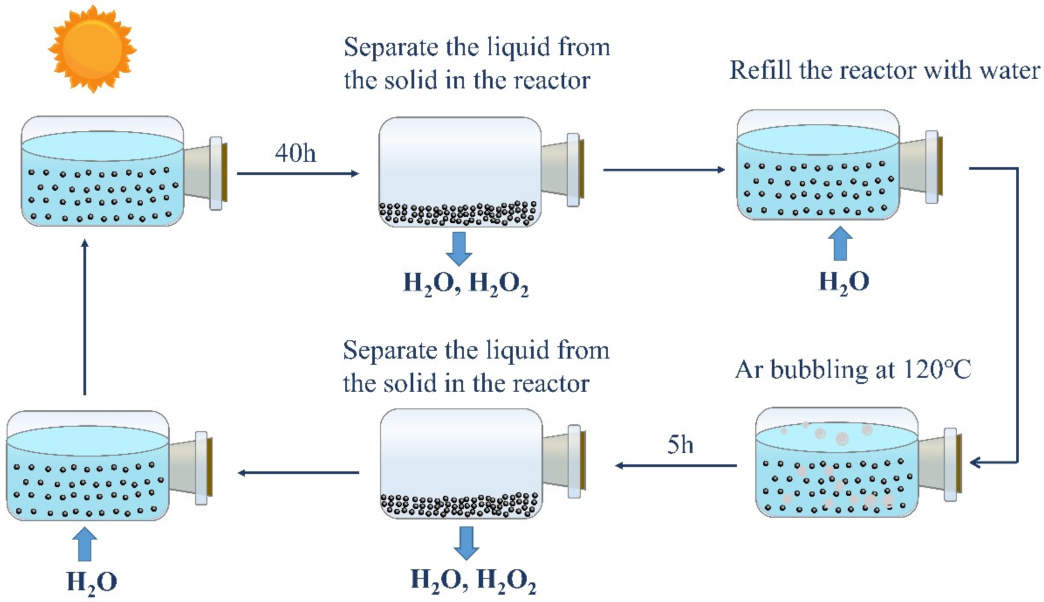

Fig. S9 Simulation diagram of in-situ photocatalyst regeneration strategy.

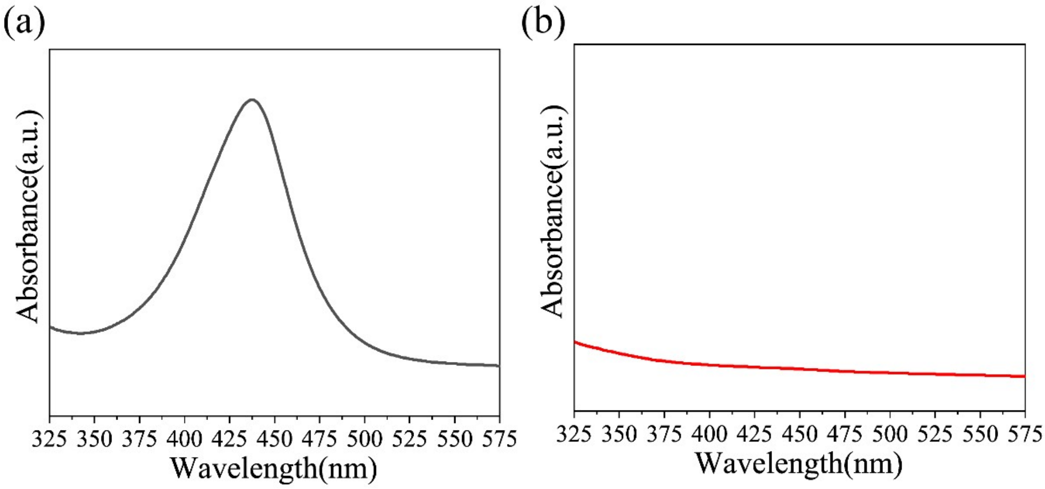

Fig. S10 The UV spectra for *o*-tolidine oxidation test of detecting peroxides. (a) the Pt/b-TiO_2 NFs photocatalyst after 40 h reaction, (b) the regenerated Pt/b-TiO_2 NFs photocatalyst. The Pt/b-TiO_2 NFs photocatalyst after 40 h reaction has strong characteristic absorption at 438 nm, indicating that H_2O_2 is adsorbed on the photocatalyst surface. The regenerated sample does not have this characteristic absorption peak, indicating that there is no H_2O_2 adsorbed on the surface of the regenerated photocatalyst.

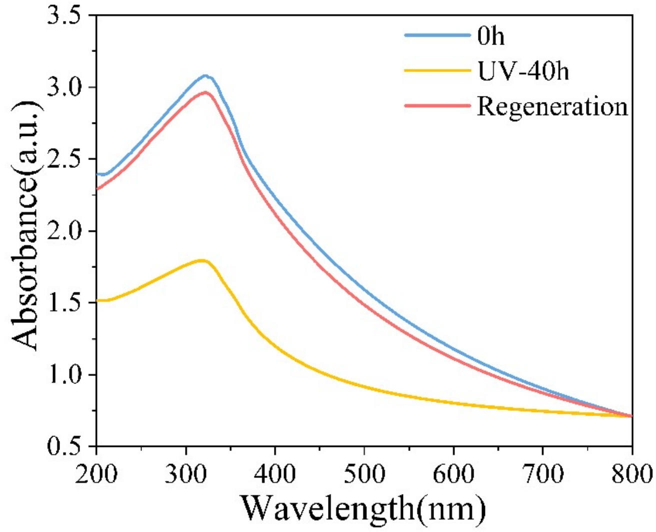

Fig. S11 UV-Vis absorption spectra of the fresh, reacted for 40 h, and regenerated Pt/b-TiO_2 NFs photocatalyst.

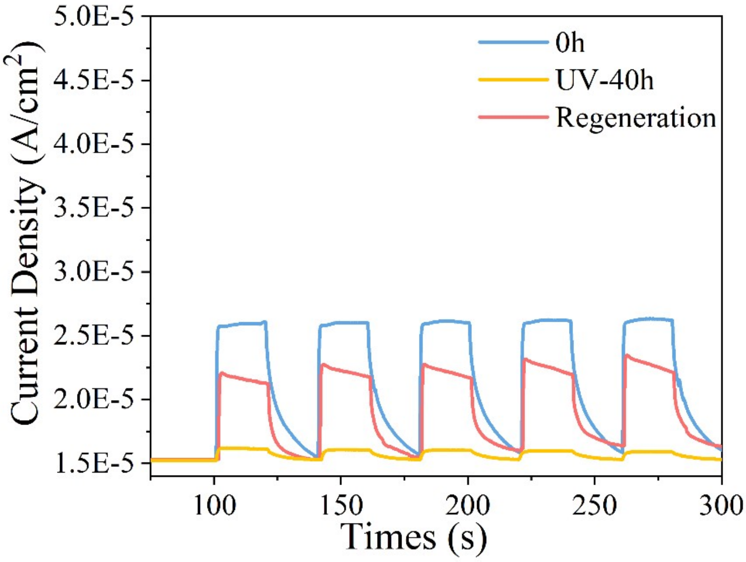

Fig. S12 Photocurrent I-t curves of the fresh, reacted for 40 h, and regenerated Pt/b-TiO_2 NFs photocatalyst.

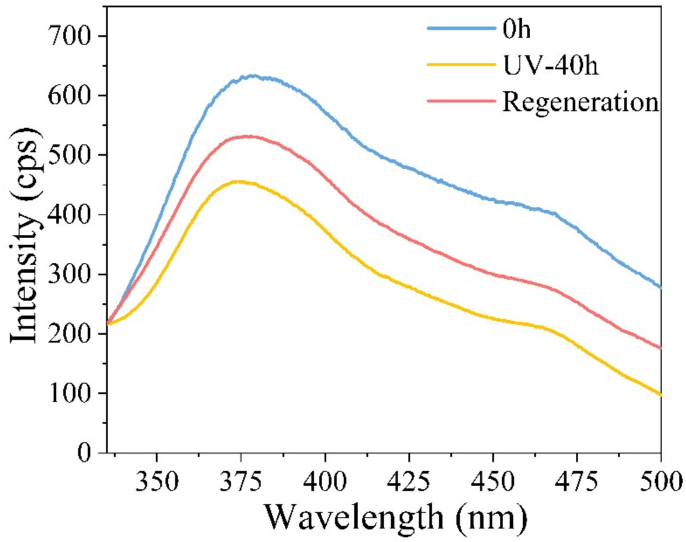

Fig. S13 Photoluminescence emission spectra of the fresh, reacted for 40 h, and regenerated Pt/b-TiO_2 NFs photocatalyst.

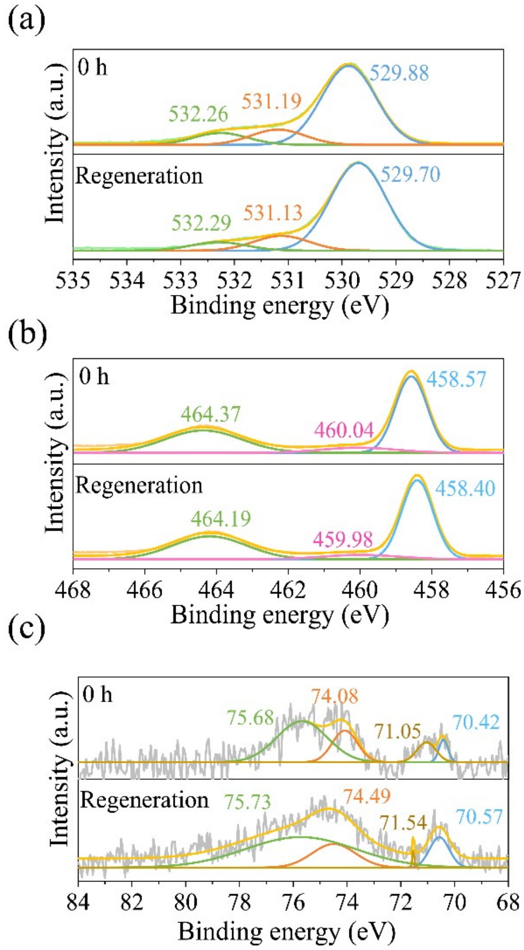

Fig. S14 XPS spectra of (a) O 1s, (b) Ti 2p and (c) Pt 4f of the fresh, reacted for 40 h, and regenerated Pt/b-TiO_2 NFs photocatalyst.

Most of the regenerated Pt could not return to the initial state, because the content of Pt^{2+} gradually increased with the progress of the photocatalytic pure water splitting reaction, and the bubbling regeneration method could not reduce the content of oxidized Pt.

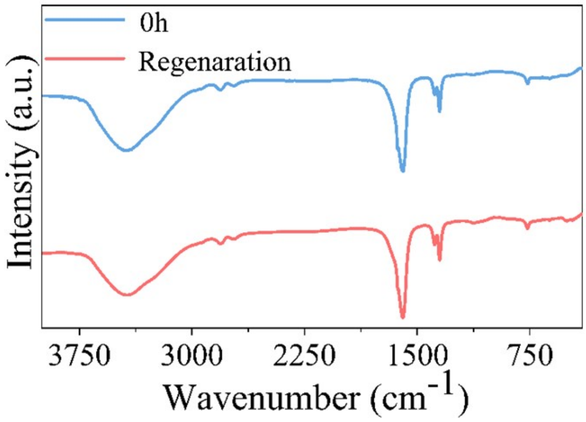

Fig. S15 FTIR spectra of the fresh, reacted for 40 h, and regenerated Pt/b-TiO_2 NFs photocatalyst.

S2. Supplementary Tables

Table. S1 Quantitative analysis of Pt/b-TiO_2 NFs after 0 h, 1 h, 20 h, and 40 h of UV light irradiation.

	Lattice oxygen (Ti-O)	**Surface Hydroxyl (Ti-OH)**	**Physisorbed Water**
0h	74.47%	14.36%	11.17%
UV-1h	63.14%	20.85%	16.01%
UV-20h	64.17%	18.37%	17.46%
UV-40h	73.15%	15.77%	11.09%
Regeneration	79.11%	13.30%	7.59%

	Ti^{4+} $2p_{5/2}$	**Ti^{3+} $2p_{5/2}$**	**Ti^{4+} $2p_{3/2}$**
0h	53.87%	8.48%	37.65%
UV-1h	68.00%	6.75%	25.25%
UV-20h	68.90%	7.95%	23.15%
UV-40h	69.56%	5.28%	25.15%
Regeneration	55.07%	7.60%	37.33%

	Pt^0 $4f_{7/2}$	**Pt^0 $4f_{5/2}$**	**Pt^{2+} $4f_{7/2}$**	**Pt^{2+} $4f_{5/2}$**
0h	5.90%	23.13%	11.07%	59.90%
UV-1h	17.44%	46.36%	0.95%	35.25%
UV-20h	13.02%	19.67%	4.06%	63.25%
UV-40h	13.02%	19.66%	4.05%	63.27%
Regeneration	11.95%	20.39%	0.71%	67.05%

Table. S2 Comparison of data on the stability of photocatalysts for photocatalytic overall water splitting. In the past three years, the highest stability time was 216 h, and 95% of them were stable for 20~30 h.

Reference	Stability	Image
Self-assembly photocatalytic reduction synthesis of graphene-encapusulated $LaNiO_3$ nanoreactor with high efficiency and stability for photocatalytic water splitting to hydrogen, Chemical Engineering Journal, 2018, 356, 580-591.	36 h	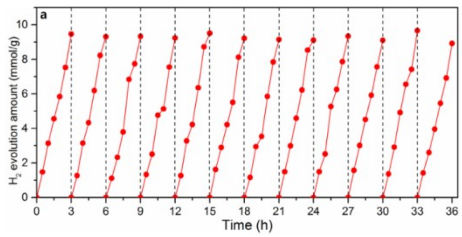
Highly efficient photocatalytic overall water splitting on plasmonic Cu_6Sn_5/polyaniline nanocomposites, Journal of Colloid and Interface Science, 2021,609, 785-793.	20 h	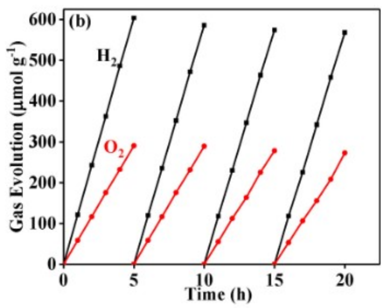
CdS@$Mg(OH)_2$ core/shell composite photocatalyst for efficient visible-light photocatalytic overall photocatalytic overall water splitting, International Journal of Hydrogen Energy, 2022, 47(14), 8729-8738.	20 h	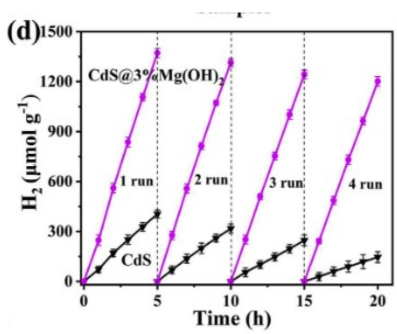

Switching from two-electron to four-electron photocatalytic pure water splitting via band bending engineering with boosted activity, Applied Catalysis B: Environmental, 2022, 305, 121054-121054.	15 h	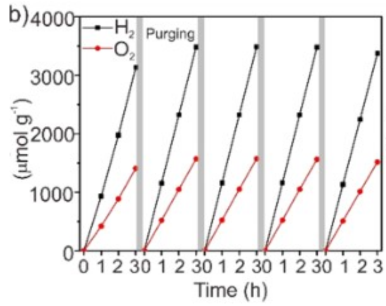
Enhanced photoelectrochemical performances in photocatalytic pollutant degradation and water splitting by direct Z-scheme $Bi_2Sn_2O_7/TiO_2$ NTAs, Ceramics International, 2022, 48(3), 3941-3953.	14 h	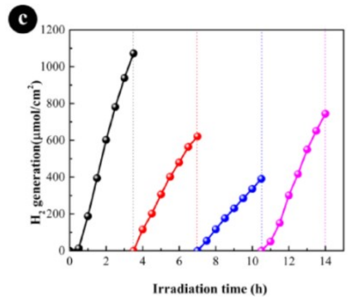
Layered g-C_3N_4/TiO_2 nanocomposites for efficient photocatalytic water splitting and CO_2 reduction: a review, Materials Today Energy, 2022, 23, 100904-100904.	25 h	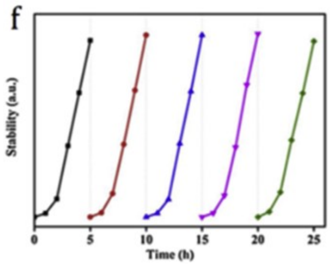
Fabrication of 0D/2D TiO_2 Nanodots/g-C_3N_4 S-scheme heterojunction photocatalyst for efficient photocatalytic overall water splitting, Applied Surface Science, 2022, 571, 151287-151287.	16 h	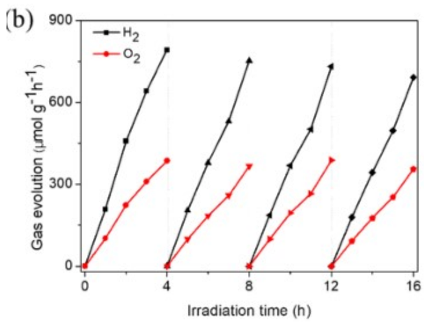
Band structure-controlled P-C_3N_4 for photocatalytic water splitting via appropriately decreasing oxidation capacity, Journal of Alloys and Compounds, 2022, 895, 162513-162513.	15 h	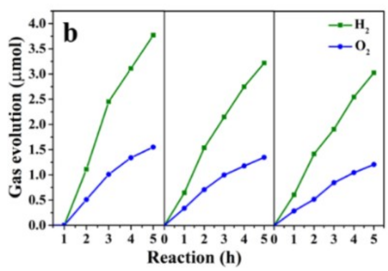

Heat treatment to prepare boron doped g-C_3N_4 nanodots/carbon-rich g-C_3N_4 nanosheets heterojunction with enhanced photocatalytic performance for water splitting hydrogen evolution, Journal of Alloys and Compounds, 2022, 898, 162846-162846.	15 h	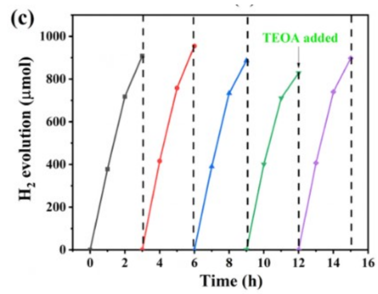
The photocatalytic overall water splitting hydrogen production of g-C_3N_4/ CdS hollow core–shell heterojunction via the HER/OER matching of Pt/ MnOx, Chemical Engineering Journal, 2021, 405, 126622-126622.	24 h	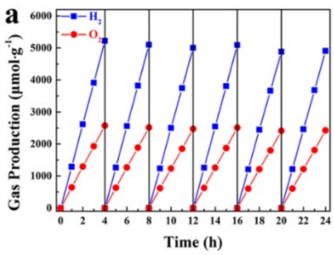
Synthesis of CdS/CoP hollow nanocages with improved photocatalytic water splitting performance for hydrogen evolution, Journal of Environmental Chemical Engineering, 2021, 9(6), 106270-106270	20 h	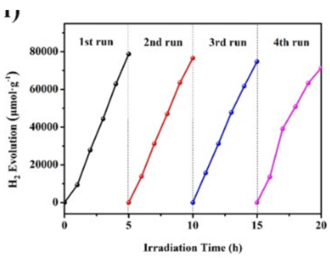
Photocatalytic hydrogen generation via water splitting using ZIF-67 derived Co_3O_4@C/TiO_2, Journal of Environmental Chemical Engineering, 2021, 9(4), 105702-105702.	20 h	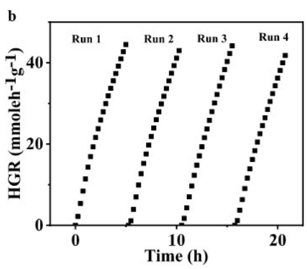

2D/2D heterostructure of ultrathin $BiVO_4/Ti_3C_2$ nanosheets for photocatalytic overall Water splitting, Applied Catalysis B: Environmental, 2021, 285, 119855-119855.	24 h	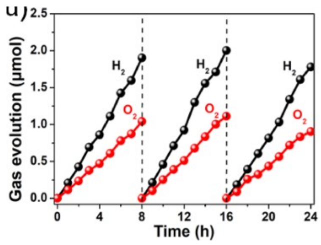
Photocatalytic overall water splitting without noble-metal: Decorating CoP on Al-doped $SrTiO_3$, Journal of Colloid and Interface Science, 2022, 606, 491-499.	9 h	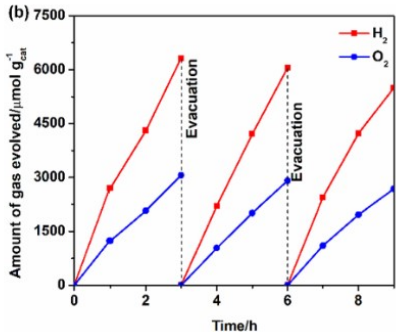
Facile synthesis of anatase/rutile TiO_2/g-C_3N_4 multi-heterostructure for efficient photocatalytic overall water splitting, International Journal of Hydrogen Energy, 2020, 45(35), 17378-17387.	12 h	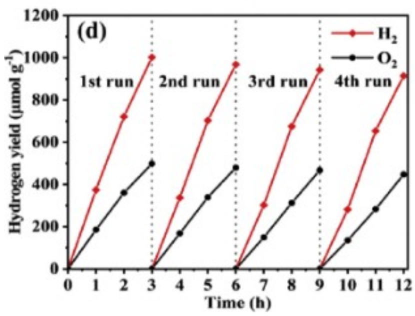
Novel Z-scheme binary zinc tungsten oxide/nickel ferrite nanohybrids for photocatalytic reduction of chromium (Cr (VI)), photoelectrochemical water splitting and degradation of toxic organic pollutants, Journal of Hazardous Materials, 2022, 423, 127044-127044.	~10 h	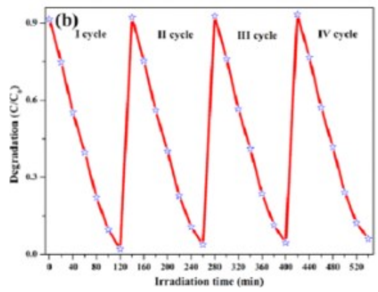

Overall photocatalytic water splitting by an organolead iodide crystalline material, Nature Catalysis, 2020, 3(12), 1027-1033.	15 h	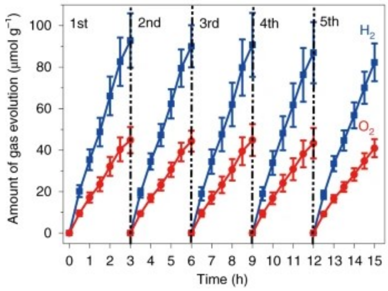
Boron-doped nitrogen-deficient carbon nitride-based Z-scheme heterostructures for photocatalytic overall water splitting, Nature Energy, 2021, 6(4), 388-397.	32 h	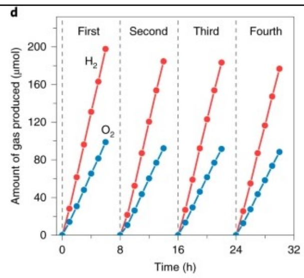
Single-atom Cu anchored catalysts for photocatalytic renewable H_2 production with a quantum efficiency of 56%, Nature Communications, 2022, 13(1), 1-10.	30 h	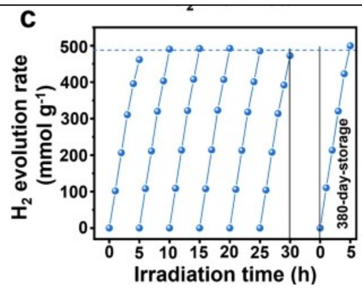
The high photocatalytic efficiency and stability of $LaNiO_3$/g-C_3N_4 heterojunction nanocomposites for photocatalytic water splitting to hydrogen, BMC chemistry, 2022, 14(1), 1-13.	20 h	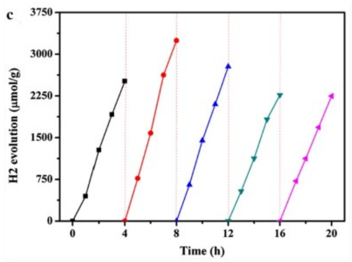
Introducing spin polarization into atomically thin 2D carbon nitride sheets for greatly extended visible-light photocatalytic water splitting, Nano Energy, 2021, 83, 105783-105783.	16 h	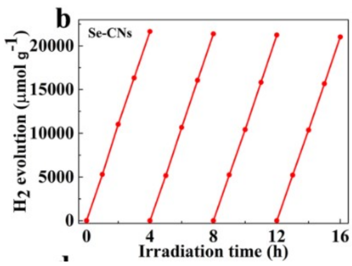
Z-scheme photocatalyst Pt/GaP-TiO_2-SiO_2: Rh for the separated H_2 evolution from photocatalytic seawater splitting, Applied Catalysis B: Environmental, 2021, 296,	16 h	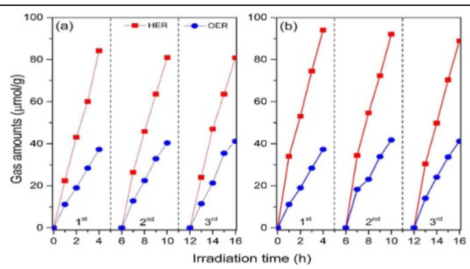

120339-120339.		
Holey defected TiO_2 nanosheets with oxygen vacancies for efficient photocatalytic hydrogen production from water splitting, Surfaces and Interfaces, 2021, 23, 100979-100979.	25 h	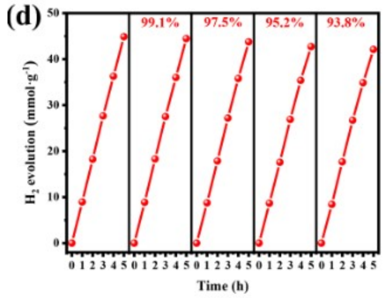
Single 2D MXene precursor-derived TiO_2 nanosheets with a uniform decoration of amorphous carbon for enhancing photocatalytic water splitting, Applied Catalysis B: Environmental, 2020, 270, 118885-118885.	16 h	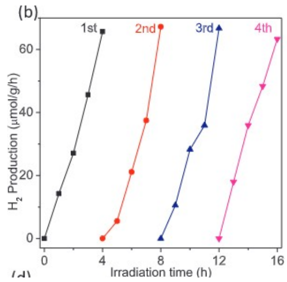
Z-scheme heterojunction through interface engineering for broad spectrum photocatalytic water splitting, Applied Catalysis B: Environmental, 2020, 267, 118661-118661.	30 h	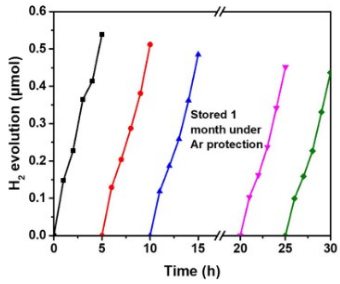
$CdS@Ni_3(NO_3)_2(OH)_4$ nanorods@nanosheets for boosted photocatalytic H_2 generation rate and stability under visible light irradiation, Colloids and Surfaces A: Physicochemical and Engineering Aspects, 2022, 639, 128352-128352.	20 h	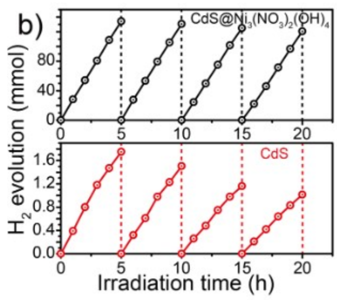

Overall water splitting on surface-polarized Sn_3O_4 through weakening the trap of Sn(II) to holes, Applied Catalysis B: Environmental, 2021, 299, 120689-120689.	15 h	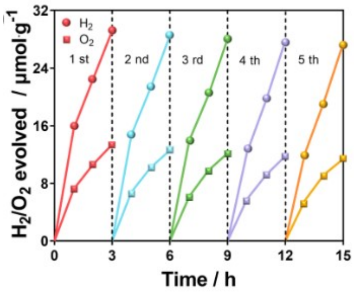
Surface-Polarity-InducedSpatialChargeSeparationBoostsPhotocatalyticOverallWater Splitting on GaN Nanorod Arrays, Angewandte Chemie, 2020, 132(2), 945-952.	9 h	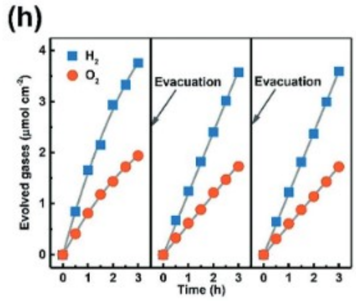
Atomically thin $PdSeO_3$ nanosheets: a promising 2D photocatalyst produced by quaternary ammonium intercalation and exfoliation, Chemical Communications, 2020, 56(41), 5504-5507.	33 h	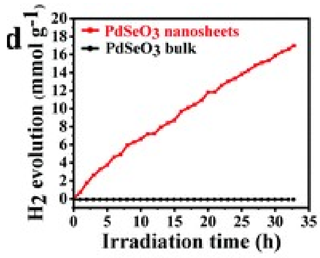
La, Al-Codoped SrTiO3 as a Photocatalyst in Overall Water Splitting: Significant Surface Engineering Effects on Defect Engineering, ACS Catalysis, 2021, 11(18), 11429-11439.	18 h	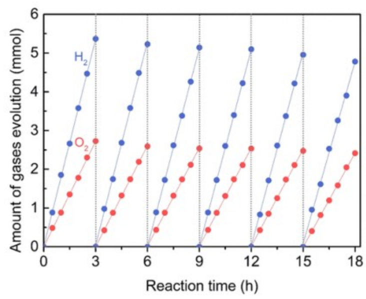
Steering Hole Transfer from the Light Absorber to Oxygen Evolution Sites for Photocatalytic Overall Water Splitting, Advanced Materials Interfaces, 2021, 8(22), 2101158-2101158.	25 h	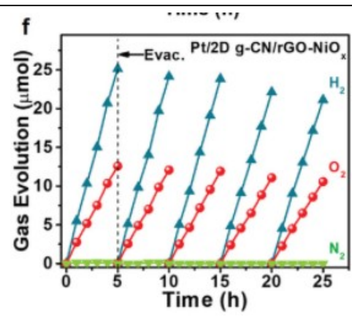

Smart Assembly of Sulfide Heterojunction Photocatalysts with Well-Defined Interfaces for Direct Z-Scheme Water Splitting under Visible Light, ChemSusChem, 2020, 13(11), 2996-3004.	42 h	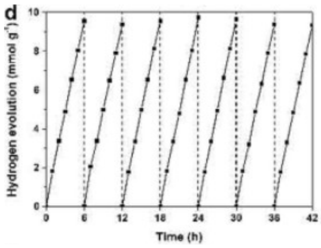
The Pt-free 1T/2H-MoS_2/CdS/MnO_x hollow core-shell nanocomposites toward overall water splitting via HER/OER synergy of 1T-MoS_2/MnO_x, Materials Today Chemistry, 2021, 21, 100528-100528.	24 h	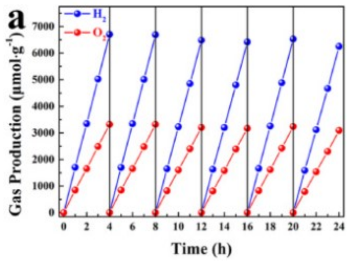
Development of BiOI as an effective photocatalyst for oxygen evolution reaction under simulated solar irradiation, Catalysis Science & Technology, 2020, 10(10), 3223-3231.	40 h	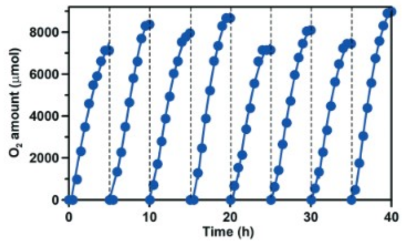
In Situ Photodeposited Construction of Pt−CdS/g-C_3N_4−MnO_x Composite Photocatalyst for Efficient Visible-Light-Driven Overall Water Splitting, ACS Applied Materials & Interfaces, 2020, 12(18), 20579-20588.	12 h	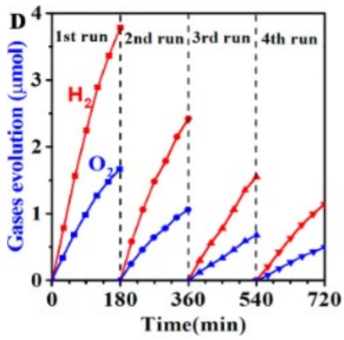
Temperature effect on green-synthesized Co_3O_4nanoparticle as photocatalyst for overall water splitting, Journal of Photonics for Energy, 2020, 10(4), 042006-042006.	12 h	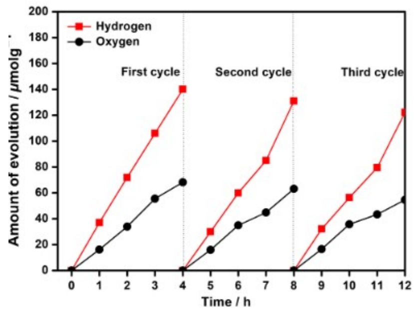

Graphitic Carbon Nitride Decorated with Nickel(II)-(3-Pyridyl) Benzimidazole Complexes and Pt Nanoparticles as a Cocatalyst for Photocatalytic Hydrogen Production from Water Splitting, ACS Applied Nano Materials, 2020, 3(11), 10659-10667.	20 h	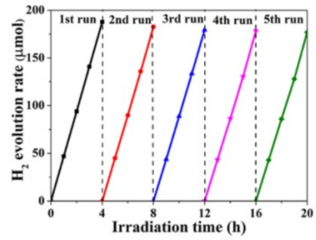
FeNi intermetallic compound nanoparticles wrapped with N-doped graphitized carbon: a novel cocatalyst for boosting photocatalytic hydrogen evolution, Journal of Materials Chemistry A, 2020, 8(6), 3481-3490.	20 h	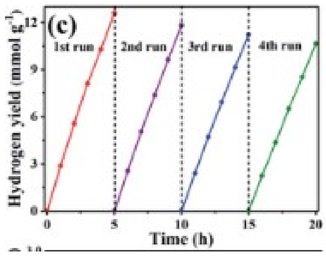
Biomass Lignin Integrated Polymeric Carbon Nitride for Boosted Photocatalytic Hydrogen and Oxygen Evolution Reactions, Molecular Catalysis, 2022, 518, 112064-112064.	25 h	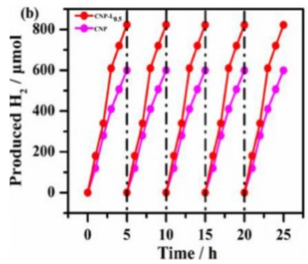
Constructing $La_xCo_yO_3$ Perovskite Anchored 3D g-C_3N_4 Hollow Tube Heterojunction with Proficient Interface Charge Separation for Stimulating Photocatalytic H_2 Production, Energy & Fuels, 2021, 35(11), 9727-9746.	16 h	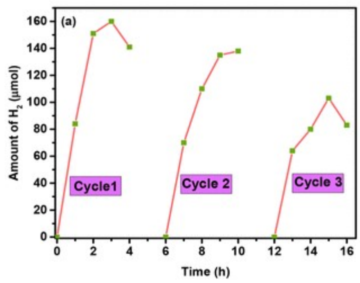

Stable and efficient Ti_3C_2 MXene/$MAPbI_3$-HI system for visible-light-driven photocatalytic HI splitting, Journal of Power Sources, 2022, 522, 231006-231006.	50 h	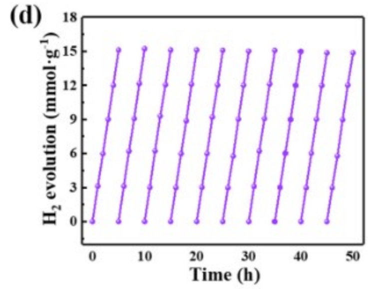
A Novel Porous Ti-Squarate as Efficient Photocatalyst in the Overall Water Splitting Reaction under Simulated Sunlight Irradiation, Advanced Materials, 2021, 33(52), 2106627-2106627.	216 h	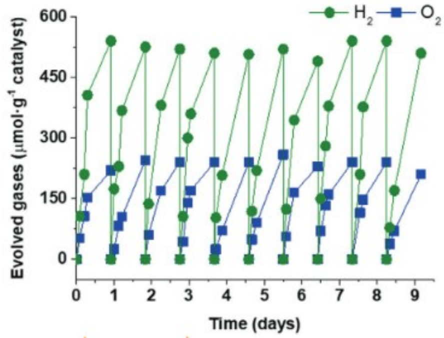
Nickel phosphonate MOF as efficient water splitting photocatalyst, Nano Research, 2021, 14(2), 450-457	110 h	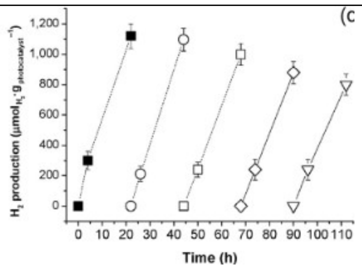
Semiconductor-based photocatalysts for photocatalytic and photoelectrochemical water splitting: will we stop with photocorrosion? Journal of Materials Chemistry A, 2020, 8(5), 2286-2322.	60 h	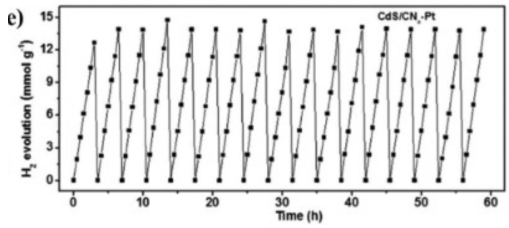
Carbon quantum dots enriching molecular nickel polyoxometalate over CdS semiconductor for photocatalytic water splitting, Applied Catalysis B: Environmental, 2021, 293, 120214-120214.	96 h